Charge separated states and singlet oxygen generation of Mono and Bis Adducts of C_{60} and C_{70}

Panagiotis Dallas [*a], Gregory Rogers [a], Ben Reid [b], Robert A.Taylor [b], Hisanori Shinohara [c], G.Andrew D.Briggs [a] and Kyriakos Porfyrakis [*a]

[a] Department of Materials, University of Oxford, Oxford OX1 3PH, UK.

[b] Department of Physics, Clarendon Laboratory, University of Oxford, Oxford OX1 3PH,UK.

[c] Department of Chemistry & Institute for Advanced Research, Nagoya University, Nagoya 464-8602, Japan

- E-mail: panagiotis.dallas@materials.ox.ac.uk; kyriakos.porfyrakis@materials.ox.ac.uk;

Keywords: Fullerenes, emission lifetimes, singlet oxygen, intersystem crossing, charge separation

Table of contents

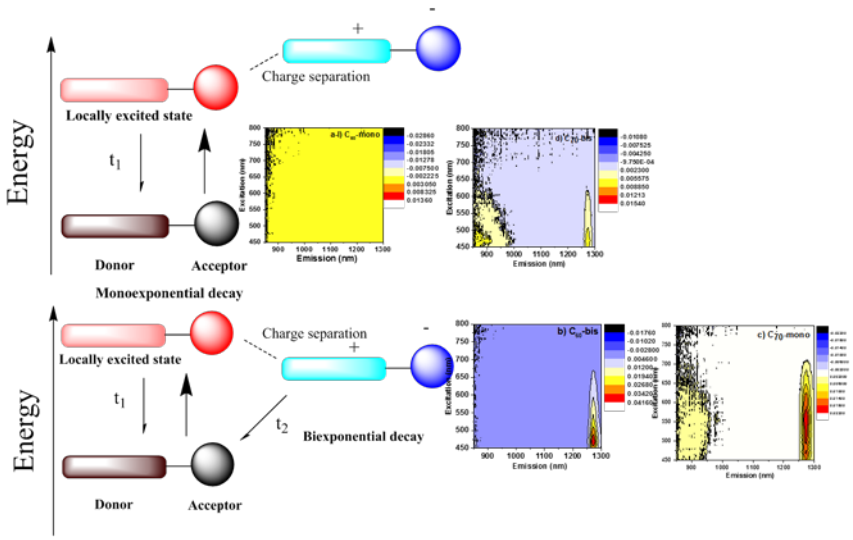

ABSTRACT:

We present a series of fullerene derivatives and a study on their photoluminescence properties, complete with their efficiency as singlet oxygen generation photosensitizers. Absorbance and emission spectra as well as the decay lifetimes demonstrate the

intramolecular charge transfer between the pyrene donor and the fullerene acceptor. The opposite effect in decay lifetime measurements is observed for the mono and bis adducts of C_{60} and C_{70} for the first time, which indicates an interplay between the charge separation and the locally excited states. A monoexponential decay was observed for the mono adduct of C_{60} and the bis adduct of C_{70}, while a biexponential decay was observed for the bis adduct of C_{60} and the mono adduct of C_{70}. This trend implies different energy transfers occurring depending on the energy levels of the fullerene cage. The quantum yields for the blue emission were 1 % and 0.12 % for the mono adducts of C_{60}-and C_{70} respectively, compared to pristine pyrene with a quantum yield of 19%. However, a four-fold increase in the yield of the red emission was observed for the mono adduct of C_{60} and two-fold decrease for the bis adduct of C_{70} compared to their pristine fullerenes. The effect of these molecules as sensitizers of the singlet oxygen radical was tested using detailed 3D excitation photoluminescence (PL) maps which demonstrated a quenching of the singlet oxygen for the C_{60}-mono and C_{70}-bis adducts while a strong photosensitizing effect was observed for the C_{60}-bis and C_{70}-mono adducts.

1. Introduction

The surface functionalization of fullerenes is a necessary step for their use in a series of applications in biomedicine as antiviral agents [1], photosensitizers [2], in solar cells as electron acceptor moieties [3] and in quantum computers [4]. The 1,3 dipolar cycloaddition firstly established by the group of Maurizio Prato [5, 6] is one of the most widely used reactions for the formation of a series of fulleropyrollidine derivatives with different anchor groups. These derivatives are easy to design and process, and have recently proved to be remarkably effective as interlayer buffer materials in organic solar cells when placed between the active layer and the cathode [7].

Fullerenes and their derivatives are known to be exceptional electron acceptors that form donor-acceptor complexes [8] and dyads [9] which exhibit photoluminescence emission, albeit with weak intensity, and an intersystem crossing (ISC) to a triplet state. Donor-acceptor dyads have been studied both experimentally and theoretically and include fullerenes linked with porphyrin [9b] or pyrene rings [10]. Detailed DFT studies on mono adducts of pyrene derivatives indicated a localization of the HOMO levels on the pyrene donor and of the LUMO on the fullerene acceptor [11]. These functional groups change the photophysical properties of the system and result in

charge separation states, different intersystem crossing lifetimes and singlet-triplet populations. This is crucial for a number of applications since the charge separated states of donor-acceptor dyads can be used for cell membrane potentials and ion transport control [12a]. The ISC renders fullerenes the most efficient known photosensitizers for the generation of the excited singlet oxygen state $^1O_2$ [13].

This combination of properties offers further potential applications as white light emitters [14] and components in quantum information processing devices [15]. However, the fluorescence in fullerenes exhibits low quantum yields because the low lying electronic transitions are only weakly allowed. Surface functionalization of fullerenes has been proven to be an effective way to control the quantum yields of the emission by and the optical patterns through lowering the symmetry of the products.

In our work we present the shift of the emission maximum and change of decay mechanism in mono and bis adducts of the two most widely used fullerenes, C_{60} and C_{70}, along with their NIR photoluminescence and singlet oxygen generation. A single pathway decay mechanism was observed in the fluorescence decay of the C_{60} mono and C_{70} bis adducts, whilst a two pathways mechanism was observed for the C_{70} mono and the C_{60} bis adducts. This is assigned to the formation of either locally excited or charge separated states. A similar effect was observed in the intensity of singlet oxygen generation as proven by its 1270 nm emission. Consequently, the materials can cover a range of emission wavelengths with photosensitizing effects that can be tuned depending on the central cage and the number of functional groups on the surface. Furthermore, the control of charge separated states in a range of organic and inorganic dyads can lead to efficient photocatalysts and light harvesting devices. [12b-12c]

2. Experimental part

2.1. Reagents: C_{60}: MER corporation, 99% purity, C_{70}: MER corporation, 95% purity, 1-pyrene carboxaldehyde: Aldrich, 99% purity, sarcosine: Aldrich, 98% purity

2.2. 1,3 dipolar cycloaddition on C_{60} and C_{70}: In a typical experiment 1-pyrene carboxaldehyde (48.3 mg-0.21 mmol for a C_{60} reaction and 1.3 mg-0.00565 mmol for C_{70}), N-methylglycine (sarcosine, 24.1 mg-0.27 mmol for C_{60} and 0.9 mg-0.01 mmol for C_{70}) and fullerenes (57.3 mg-0.08 mmol for C_{60} and 2.24 mg-0.00266 mmol for C_{70}) were dissolved in 90 ml (20 ml for C_{70}) of toluene. The reaction proceeded under nitrogen flow at 110 ^oC.

2.3. Purification and isolation of the products: The mono and multi-adducts were isolated by HPLC using a BuckyPrepM column. The flow rate was 16 ml/min and toluene was used

as the eluent phase. The purification is a multi-step process: First the reaction mixture was separated into fractions with broadly similar retention times with the peaks corresponding to the 1-pyrene carboxaldehyde and the fullerene discarded at this point. These fractions were then further purified by recycling HPLC. Each sample was recycled five times to achieve a good resolution between peaks before each distinct product was isolated.

2.4. Concentrations and quantum yield methodology: The concentration for the PL and ultraviolet (UV)-Visible measurements used to estimate the quantum yield (QY) were: Pyrene: 10^{-6}g/ml in either toluene or ethanol, pristine C_{60}: $3\cdot10^{-5}$ g/ml, pristine C_{70}: $0.67\cdot10^{-5}$ g/ml, C_{60}-mono: $3\cdot10^{-5}$ g/ml, C_{70}-mono: $3.17\cdot10^{-5}$ g/ml. The quantum yield of C_{60} and its derivatives were recorded against pyrene. Based on the well-known pyrene QY of 0.65 in ethanol we calculated the QY in toluene as 0.19 and then based on this value we estimated the quantum yields under 335 nm excitation. For fullerenes the quantum yield value of $2.2\cdot10^{-4}$ for C_{60} and $5.4\cdot10^{-4}$ for C_{70} under 520 nm excitation were taken as references and a correction using the refractive index of ethanol and toluene was performed based on previously published works [16]. The following spectral ranges were used: Pyrene in toluene: 325-346 nm, Pyrene in ethanol: 325-346 nm, Pristine C_{60}: 500-650 nm (exc. 520 nm), Pristine C_{70}: 421-540 (exc. 520 nm), C_{60}-mono: 325-346 nm (exc. 335 nm), 500-650 (exc. 520 nm), C_{70}-mono: 325-346 nm (exc. 335 nm), 421-540 (exc. 520 nm)

3. Characterization techniques

The samples were purified by HPLC chromatography using a Buckyprep M silica column, 20 × 250 mm. Toluene was used as the eluent phase and the flow rate was 16 ml/min for all experiments. UV-Vis-(NIR) spectra were recorded on a Jasco 570 spectrometer using quartz cuvettes. Excitation dependence photoluminescence maps and steady state spectra were recorded on a Jasco FP6200 and a ISA Fluoromax-2 Fluorimeter in toluene and chloroform solutions. Matrix-assisted laser-desorption ionization time-of-flight mass spectra (MALDI-TOF MS-negative ionization) were obtained from a Bruker Ultraflex III MALDI-TOF spectrometer using trans-2-[3-(4-tert-Butylphenyl)-2-methyl-2-propenylidene] malononitrile (DCTB) as a matrix. NMR spectra were recorded on a Bruker 400 MHz with CS_2/$CDCl_3$ (20:80 v/v).

4. Results and discussion

4.1. Synthesis and purification

We attached a second photoluminescence moiety, an electron donating pyrene ring, through 1,3 dipolar cycloaddition of 1-pyrene carboxaldehyde and sarcosine to the surface of fullerenes. We chose two different fullerene cages, C_{60} and C_{70}, and studied their photoluminescence properties under high energy and low energy excitations targeted to the pyrene ring and the fullerene cage respectively. We used HPLC to isolate the different adducts for both C_{60} and C_{70}, and identified the structures through mass spectroscopy and ^{1}H NMR spectroscopy. Figure 1a shows the full HPLC traces for both fullerenes. For the PL study we isolated the C_{60} and C_{70} mono adducts (abbreviated as C_{60}-mono and C_{70}-mono) and bis adducts of each. Based on the ^{1}H NMR (Figure S11) and the UV-Visible data, the bis adduct of C_{60} is identified as a mixture of the trans-3 and equatorial isomers. This agrees with previously published data on different fulleropyrolidines [17], with an up-field chemical shift in the pyrolidine protons due to the presence of electron donating pyrene groups. In the case of C_{70}, the presence of a doublet at the same chemical shift in both mono and bis adducts, combined with their very similar HPLC retention time (Figure 1) indicates the presence of the trans-1 isomer [17]. However, the detailed PL spectroscopic analysis revealed no isomeric differences.

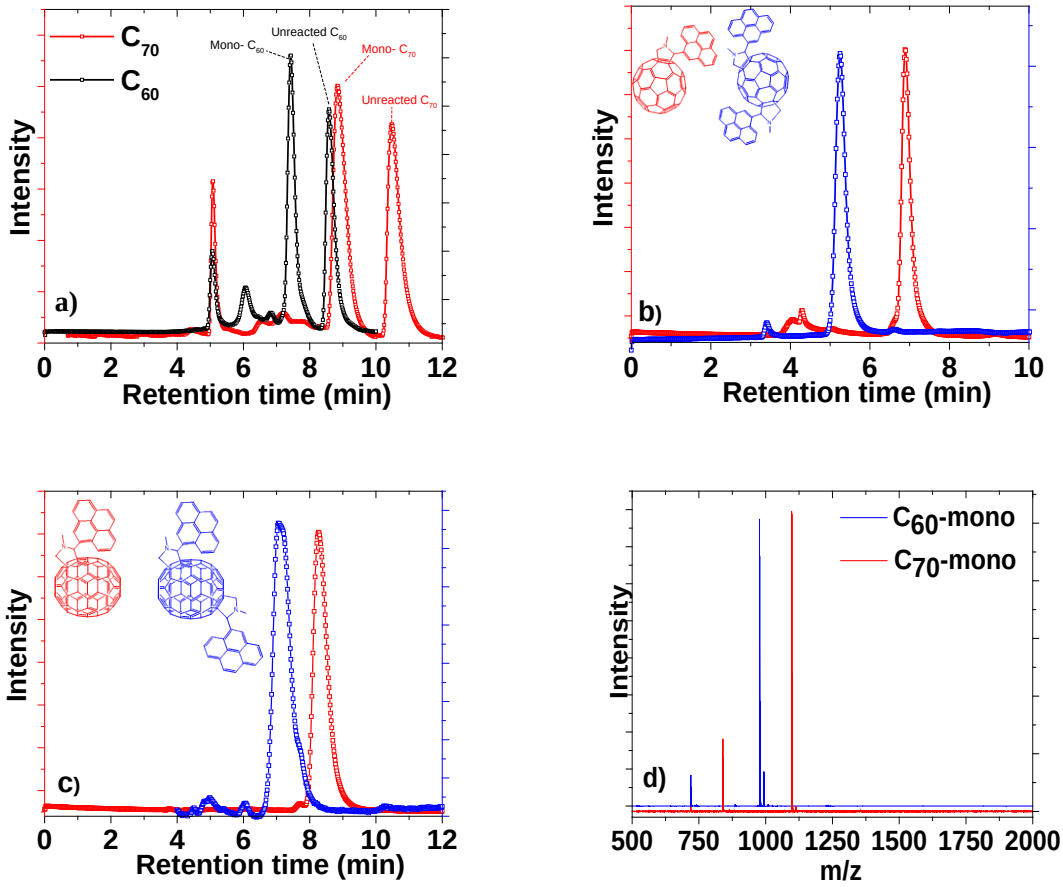

Figure 1. a) HPLC chromatographs of the reaction mixture of C_{60} and C_{70}. HPLC of the purified mono and bis adducts of C_{60} (b) and C_{70} (c). d) Mass spectrometer spectra for the mono adducts of C_{60} and C_{70}. The mass spectra of the bis adducts are given in the supporting information.

4.2.UV-Visible absorbance

The UV-Visible absorbance spectra of the mono and bis-adducts in toluene are presented in Figure 2. The pyrene absorbance peaks centered at 396, 375 and 365 nm (see Figure 2) for 1-pyrene carboxaldehyde are blue-shifted to between 350 nm and 332 nm for all of the C_{60} and C_{70} mono and bis adducts. This blue-shift is due to the anchoring of the aromatic ring to the fullerene cage and the energy transfer that takes place between them under photo-excitation [13]. The absence of the lowest energy 400 nm absorbance peak of the pyrene carboxaldehyde in all derivatives [18] proves the absence of any physisorbed unreacted dye molecules. The intramolecular interactions between the fullerene and pyrene (acceptor and donor) groups will be more clearly demonstrated by the PL data [19]. The absorbance pattern in the UV range is similar for all adducts (Figure 2). For C_{60}-mono the typical small peak for fulleropyrrolidine derivatives is observed at 430 nm [20]. The C_{70} derivatives provide the most obvious blue-shift and quenching of the 472 nm pristine

fullerene peak. This peak is quenched to an even greater extent when moving from the mono adduct to the bis adducts. These observations in the visible range absorbance imply a disruption of the fullerene surface conjugation, as indicated by the blue-shift of the absorbance and its decreased intensity.

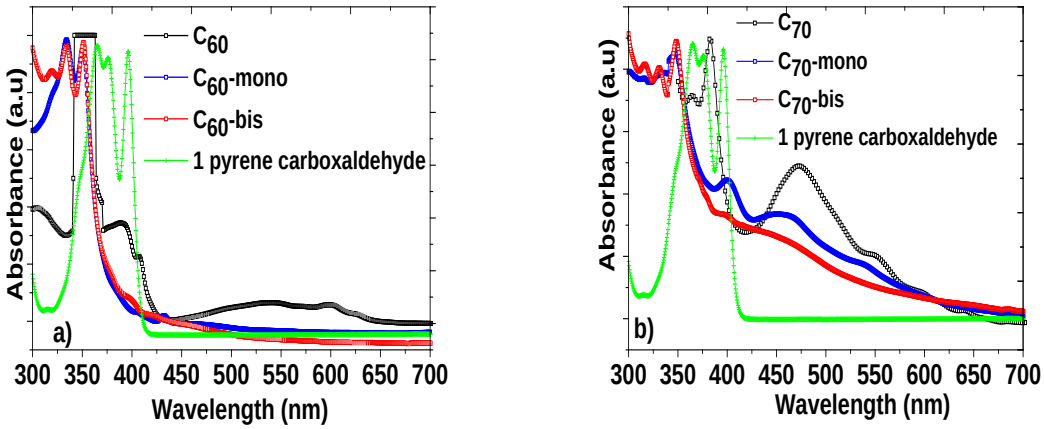

Figure 2. UV-Visible absorbance spectra of the mono and bis-adducts of (a) C_{60} and (b) C_{70}, in toluene solutions. Green: the 1-pyrene carboxaldehyde precursor. The UV-Visible absorbance spectra of pristine pyrene in both ethanol and toluene exhibiting two peaks at 323 and 336 nm and is presented in Figure S3.

4.3.Photoluminescence spectra under high energy (300-450 nm) excitations

We now turn our attention to the photoluminescence properties of our samples. The optimum solvent with the highest PL intensity for 1-pyrene carboxaldehyde is ethanol and exhibits minor solvatochromic effects typical of aromatic dyes and have been reported previously for pyrene derivatives in a series of polar and aliphatic solvents [21]. The maximum wavelength (λ_{max}) of the peak that we observed in ethanol and toluene is in accordance with a previous study by Lianos et al for this chromophore. For clarity we present the excitation dependence photoluminescence maps for both pyrene (Fig.3a, $\lambda_{exc=}$352 nm, $\lambda_{em=}$392 nm) and 1-pyrene carboxaldehyde (Fig.3b, $\lambda_{exc=}$335 nm, $\lambda_{em=}$417 nm). Due to the absence of a polar group that can further conjugate to the aromatic ring the pattern of the pristine pyrene appears significantly simpler with smaller Stokes shifts than the 1-pyrene carboxaldehyde and with identical patterns both in ethanol and toluene (see S.I.Fig.S2).

The photoluminescence of the pyrene fluorophore is a very complicated process that depends on the solvent, the functionalization and the dielectric environment. It gives rise to vibrational features and to the formation of an excited dimer, the excimer (D_e) which competes with the excited monomeric fluorophore (D_m). The rate constants of the equilibrium

between these two states depend on both the radiative (k_r) and non-radiative (k_{nr}) pathways and has been found to be strongly depend on the molecules surrounding the pyrene, for example surfactants in micellar aqueous solutions [22]. Usually, this excimer emission appears at 460 ([22b] or 500 nm [22a] compared to a monomer peak at 370-400 nm and can be seen in the spectrum of 1-pyrene carboxaldehyde in Figure 3b. Furthermore, pyrene shows a number of vibronic bands strongly depending on the polarity and the nature of its microenvironment and the groups that are anchored to it. [22b-c] In the systems that we study the fluorophore is connected with two large graphitic buckyballs with different symmetries and vibrational modes hence it is expected that the excited states of pyrene would be strongly dependent on the fullerene cage.

We subsequently recorded the photoluminescence maps initially in toluene solutions for both the C_{60} and C_{70} mono and bis-adducts. C_{60} mono and bis adducts display a double peak maximum pattern signaling significant vibronic effects in the spectrum. (Figure 3c-f). The pattern appears to be inverted between the two adducts. In the case of C_{70} the patterns do not show the inversion of the fine features as observed in the C_{60} adducts. Here we note that the C_{70} cage has a lower symmetry than C_{60} [23] with a significantly more complicated Raman spectrum and the adducts during the 1,3 dipolar cycloaddition are preferentially substituting the polar region of the ovoid C_{70} cage [24]. Due to the significant symmetry breaking of the cage we observe an intra-level transition for C_{60}-mono with two maxima at 409 and 432 nm for 377 nm excitation and an inter-level transition for the C_{60}-bis with optimum vibrational level for radiative decay to be reached with two different wavelengths. We plot these transition alongside a proposed excimer formation scheme for the pristine pyrene in Figure 4. Similar inverted patters were observed for the C_{70} adducts. But in the case of C_{70} they were observed in the red region (em.650-750 nm) under 470-500 nm excitation and they will be later discussed. We recorded the same photoluminescence maps in chloroform solutions and are presented in the S.I. and will be discussed in Chapter 4.4.

Under 405 nm laser illumination, the pristine fullerenes and C_{70}-mono do not show any visible luminescence. Indeed the quantum yield of the C_{70}-mono is lower than the pristine C_{70} and is not visible with the naked eye. However, the C_{60}-mono and C_{60}-bis adducts show a bright blue emission, similar to the PL spectra. Finally the C_{70}-bis adducts show a luminescence with a color more difficult to distinguish visibly due to a combination of multiple emissions in the visible range. All images are shown in Figure 3c.

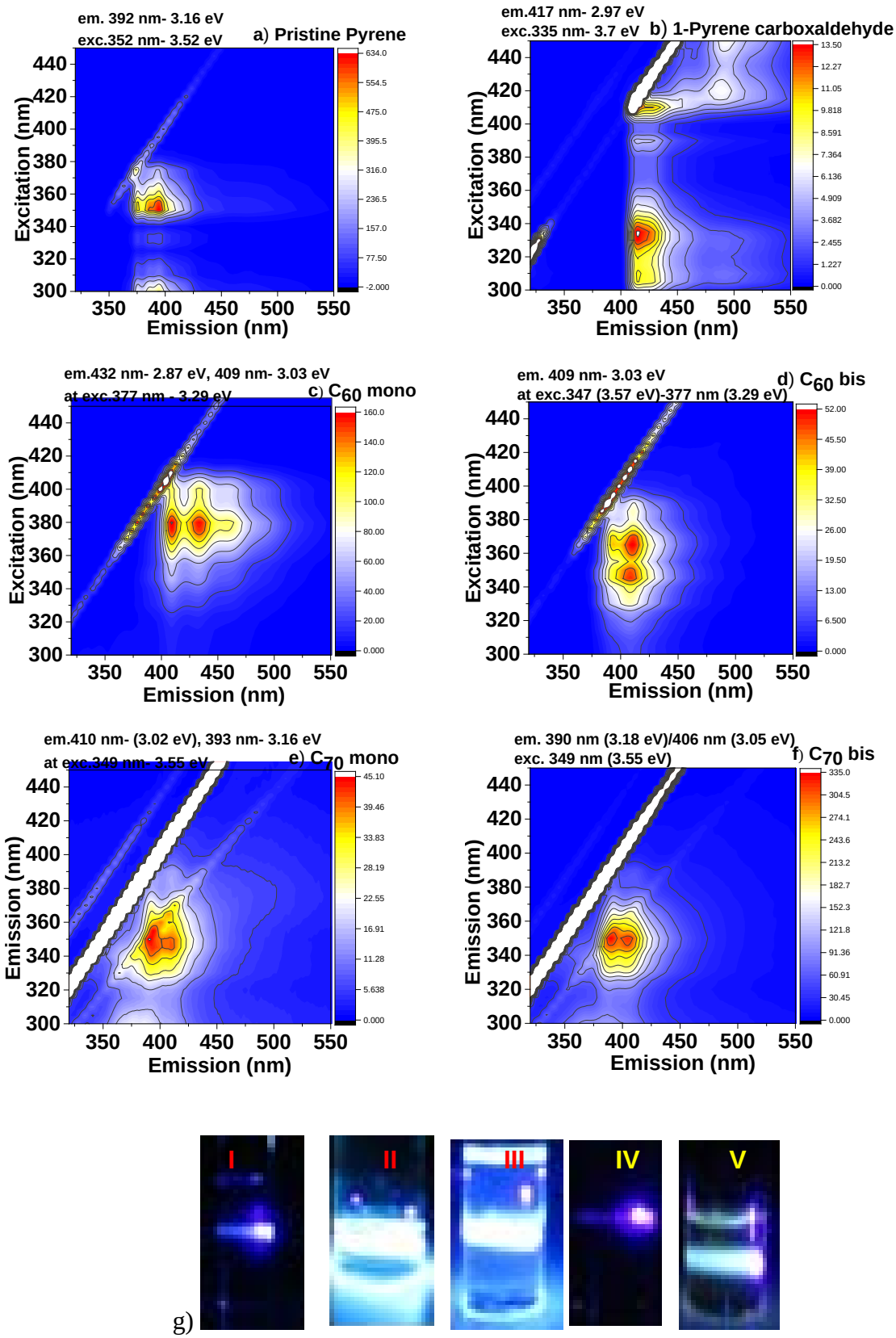

Figure 3. Photoluminescence excitation dependence spectroscopy maps in toluene (in chloroform see Fig.S12) correspond to the high energy S_1-S_0 for a) Pristine pyrene b) Pristine 1-Pyrene carboxaldehyde c) C_{60}-mono d) C_{60}-bis e) C_{70}-mono f) C_{70}-bis derivatives. g) Images taken under 405 nm laser for I) C_{60} II) C_{60}-mono III) C_{60}-bis IV) C_{70}-mono V) C_{70}-bis.

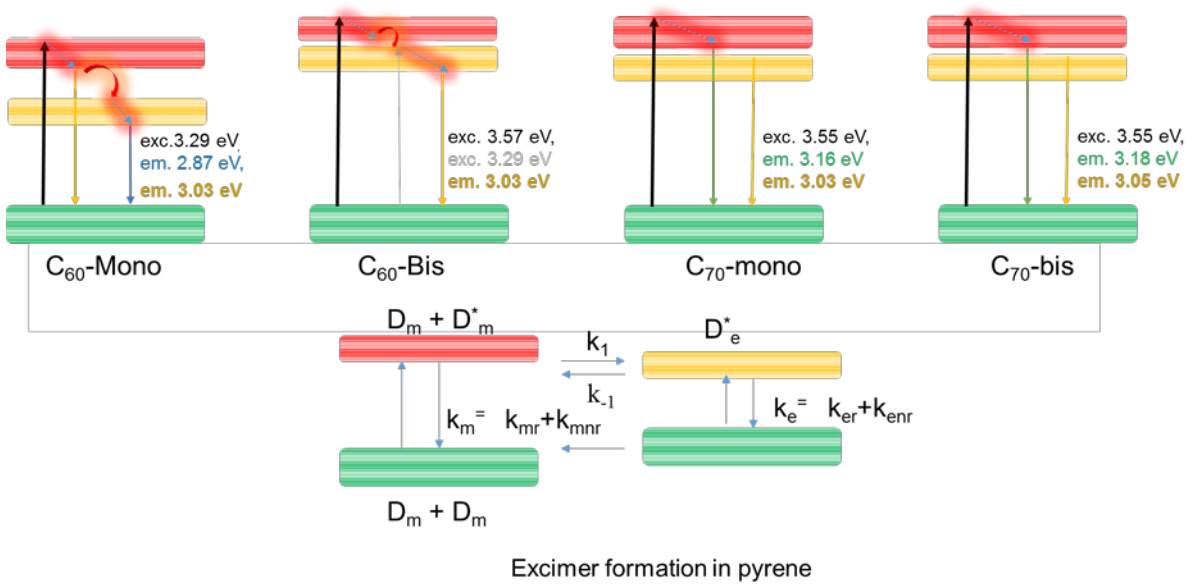

Figure 4. The excitation and decay pathways for all fullerene adducts and a scheme of the excimer formation in pyrene. D_e: excimer, D_m: monomer, k_{mr}, k_{mn}: radiative and non-radiate decay constants.

4.4.Time resolved photoluminescence ($\lambda_{exc=}$395 nm)

To further study the nature of these emissions and the intramolecular interactions in the pyrene-fullerene molecules we recorded the photoluminescence lifetimes under 395 nm laser excitation. The decay plots and the fluorescence lifetimes are presented in Figure 4. In both C_{60} and C_{70} (Figure 5) the time resolved spectra recorded for higher emission wavelengths give rise to longer fluorescence lifetimes and a lower intensity of fluorescence. In C_{60} the bis adducts have a biexponential decay and longer decay lifetimes while the mono adducts to have a monoexponential decay and shorter decay lifetimes. The opposite effect is observed in the C_{70} mono and bis adducts with the C_{70}-mono adduct to have a biexponential decay and the bis adduct a mono exponential decay. We summarize all the lifetimes in Table 1. The biexponential decay indicates two different decay mechanisms and the difference between C_{60} and C_{70} can be assigned to the different energy levels and symmetry present in the two fullerenes. In Figure 6 we present the HOMO LUMO levels of C_{60}, C_{70} and pristine pyrene with the degenerate h_u and t_{1u} orbitals. According to previous electrochemical studies the HOMO LUMO levels in solution based on the oxidation potentials are 2.32 and 2.22 V for C_{60}, C_{70} respectively.

Previous works on donor-acceptor systems indicated that the presence of a biexponential decay is due to the formation of a charge separated state with a longer lifetime. This is in addition to a locally excited state with a shorter lifetime [9]. In the case that the charge

separated state lies higher in energy than the locally excited state, the charge separated state will not be populated and only a mono exponential decay is observed. Due to different symmetry and energy levels of the C_{60} and C_{70} cages this charge separation state is favorable with a different number of pyrene groups in each system. Locally excited states have been also observed in small molecular chromophores and have been described as a low energy excitation of bond-pairing degrees of freedom closer to the ground state state. [25] In various fluorophores, the charge transfer processes and charge separated state are dependent on the dielectric environment, in our case the solvent molecules. [26] To that end we recorded the excitation dependent photoluminescence maps in chloroform which has a significantly higher dielectric constant (4.8) compared to toluene (2.2) and is also a very good solvent for our system. Indeed the C_{60}-mono and C_{70}-bis adducts gave identical (C_{60}) or nearly identical spectra with the same Stokes shifts, in contrast the C_{60}-bis and C_{70}-mono demonstrated some differences in the photoluminescence maps. We present all the excitation and emission mapping spectra in Fig.S12. More specifically, the C_{60}-bis adduct is demonstrating a loss of the vibronic in nature fine spectral features, while the C_{70}-mono is exhibiting a red shift of the excitation spectrum by 17 nm and of the emission spectrum by 7 nm with a significant expansion of the spectrum tail towards higher wavelengths.

As a comparison, we recorded the time resolved fluorescence of the parent molecule, the precursor 1-pyrene carboxaldehyde. The 1-pyrenecarboxaldehyde exhibits two fluorescence maxima with a weak fluorescence at 552 nm which has a lifetime of 14 ns (Figure 5c, red trace). This long lived emission is not present in our fullerene adducts, indicating an intramolecular charge transfer from the pyrene donor to the fullerene acceptor takes place instead of the pyrene intersystem crossing. Due to the sensitivity limits of our detector, we were not able to record the photoluminescence lifetimes at wavelengths longer than 600 nm.

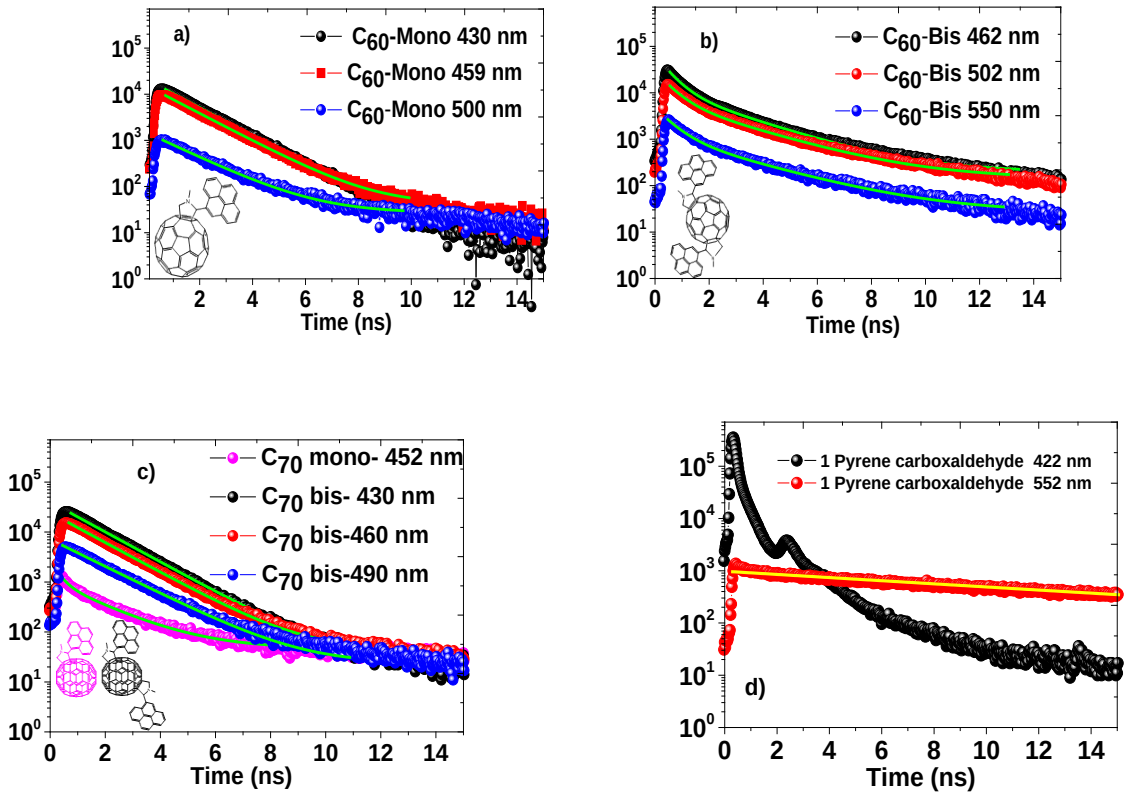

Figure 5. Photoluminescence lifetime measurements under 395 nm laser excitation for a) C_{60}-mono, b) C_{60}-bis, c) C_{70}-mono and bis and d) 1-Pyrenecarboxaldehyde. The artefact in at 2.2 ns (black line) is due to electrical reflection. The instrument response function (120 ps is given in S.I. for clarity). The emission maximum is indicated in the graph legend for the fullerene adducts and the pyrene precursor. [30] In C_{60}-bis and C_{70}-mono adduct two different lifetimes were deduced from their biexponential decay mechanism. For the C_{60}-mono and C_{70}-bis a monoexponential decay was observed. Each data set was fitted with the equation y = A1*exp(-x/t1) for the monoexponential systems and y = A1*exp(-x/t1) + A2*exp(-x/t2) + y0 for the biexponential systems. The fitted curves are shown as green lines. The residual fitting data are given in S.I., Fig.S13.

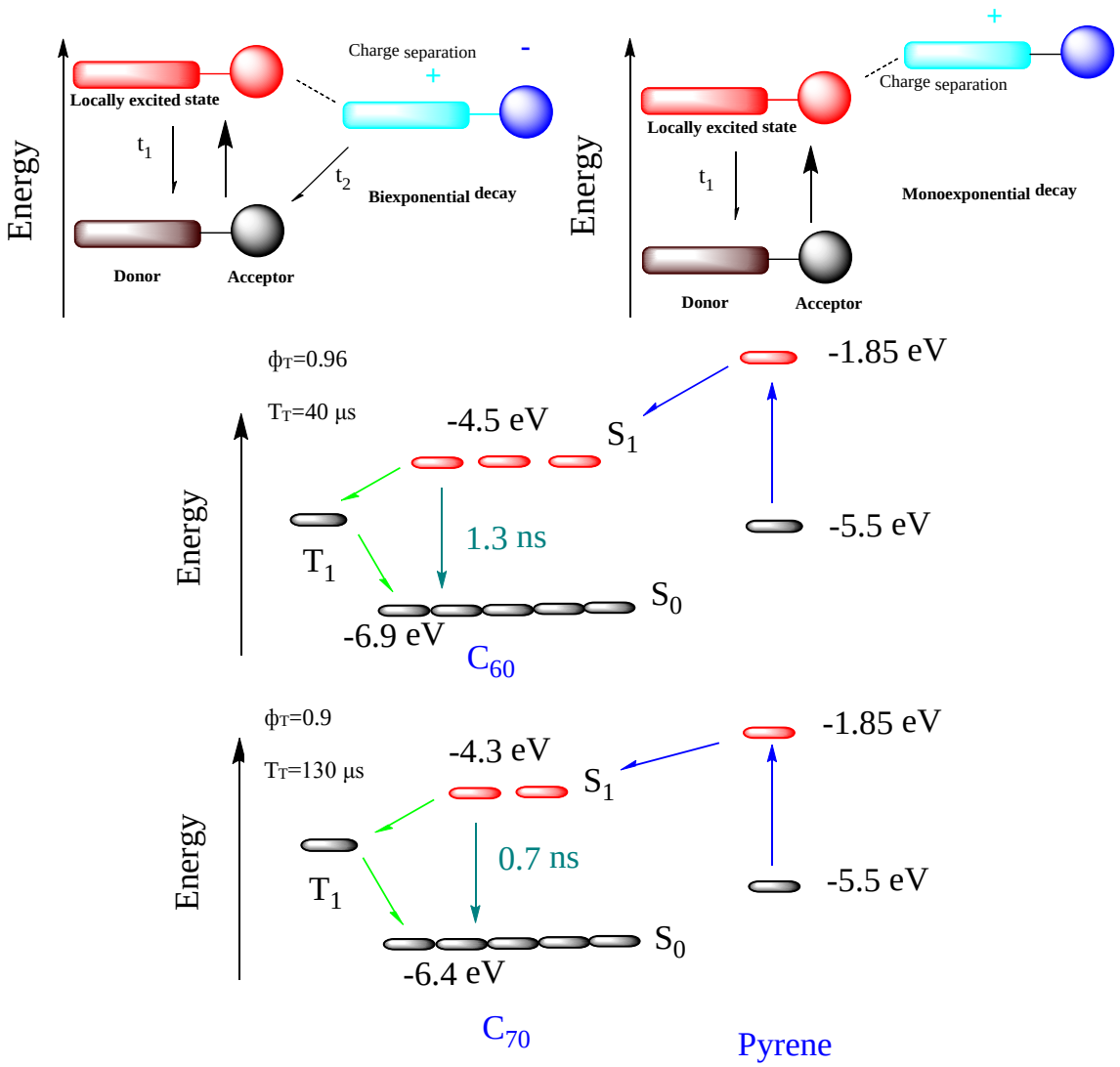

Table 1.

Sample	t_1 (ns)	t_2 (ns)	Sample	t_1 (ns)	t_2 (ns)
C_{60} mono 430 nm	1.43	N/A	**C_{70} mono 452 nm**	0.27	1.71
C_{60} mono 459 nm	1.50	N/A	**C_{70} bis 430 nm**	1.44	N/A
C_{60} mono 500 nm	1.68	N/A	**C_{70} bis 460 nm**	1.47	N/A
C_{60} bis 462 nm	0.54	2.54	**C_{70} bis 490 nm**	1.62	N/A
C_{60} bis 502 nm	0.63	2.89	**C_{60} bis 550 nm**	0.64	3

Figure 6. A schematic representation of the locally excited and charge separated states and the energy levels, singlet and triplet state lifetimes of C_{60}, C_{70} and pristine pyrene. [27] In **Table 1** we present the lifetime values of the different derivatives as estimated by the time resolved fluorescence spectroscopy. The shorter lifetime corresponds to the locally excited state [9c]

4.5.Photoluminescence under low energy (450-530 nm) nm excitations

When the fullerene cages are illuminated by light at 488 nm, where the excitation targets the carbon cage, emissions are seen in the far red/NIR regions of the spectrum (Figure 7). In general the photophysics of the fullerenes are governed by slow radiative transitions and an intersystem crossing to the triplet state, resulting in low quantum yields and weak emissions in the far red region [28]. However, the addition of groups to the surface changes these properties. The blank toluene spectra displays the inelastic scattering, resulting in an excitation dependent wavelength which sometimes is erroneously attributed to radiative decay. These peaks, with constant spacing of 3000 cm^{-1} are shown in Figures S4-5. As such the data sets presented here are the radiative decays resulting in fluorescence.

We recorded the detailed excitation dependence photoluminescence maps for the pristine fullerene, the mono and the bis adducts (Figure 7). The typical excitation independent broad and low intensity emission with λ_{max} centered at 715 nm (1.734 eV) was observed for the pristine C_{60} and corresponds to the $S_1 \rightarrow S_0$ transition with an optimum excitation wavelength λ_{ex}=495 nm (2.5 eV) [29-30]. This emission was slightly shifted and became narrower for the mono and bis C_{60} adducts with λ_{max} at 711 (1.740 eV) and 719 nm (1.724 eV) respectively. Furthermore, the optimum λ_{ex} was now shifted to higher energy levels at 470 (2.637 eV) and 467 nm (2.655 eV) respectively, signaling an effect in the energy levels due to the pyrene anchor groups. Similar small shifts in this $S_1 \rightarrow S_0$ transition have been previously reported on other substituted C_{60} adducts which do not contain a fluorescent pyrene ring [31]. This work assigned the increase in fluorescence upon addition of a functional group to a decrease in the rate of intersystem crossing. This decrease is due to the change of symmetry from I_h (C_{60}) to C_{2v} (monoadducts) or C_1, C_2 or Cs symmetries for the different bisadducts [30]. Previously, the addition of six pyrolidine rings led to an increase in the emission intensity [29]. This was attributed to a reduction of conjugation within the fullerene core, leading to higher excitation energies and larger single-triplet gaps. It was also claimed that a blue-shift in the spectrum and a reduction of the excited-state $S_1 \rightarrow T_1$ intersystem crossing are a result of the energy level and symmetry change [13], with a photoinduced intramolecular energy transfer between the donor and the acceptors taking place in such dyads [32]. This energy transfer has been shown to proceed from the first excited singlet state of the pyrene donor to the S1 state of the fullerene acceptor in fullerene-pyrene mono-adducts [33].

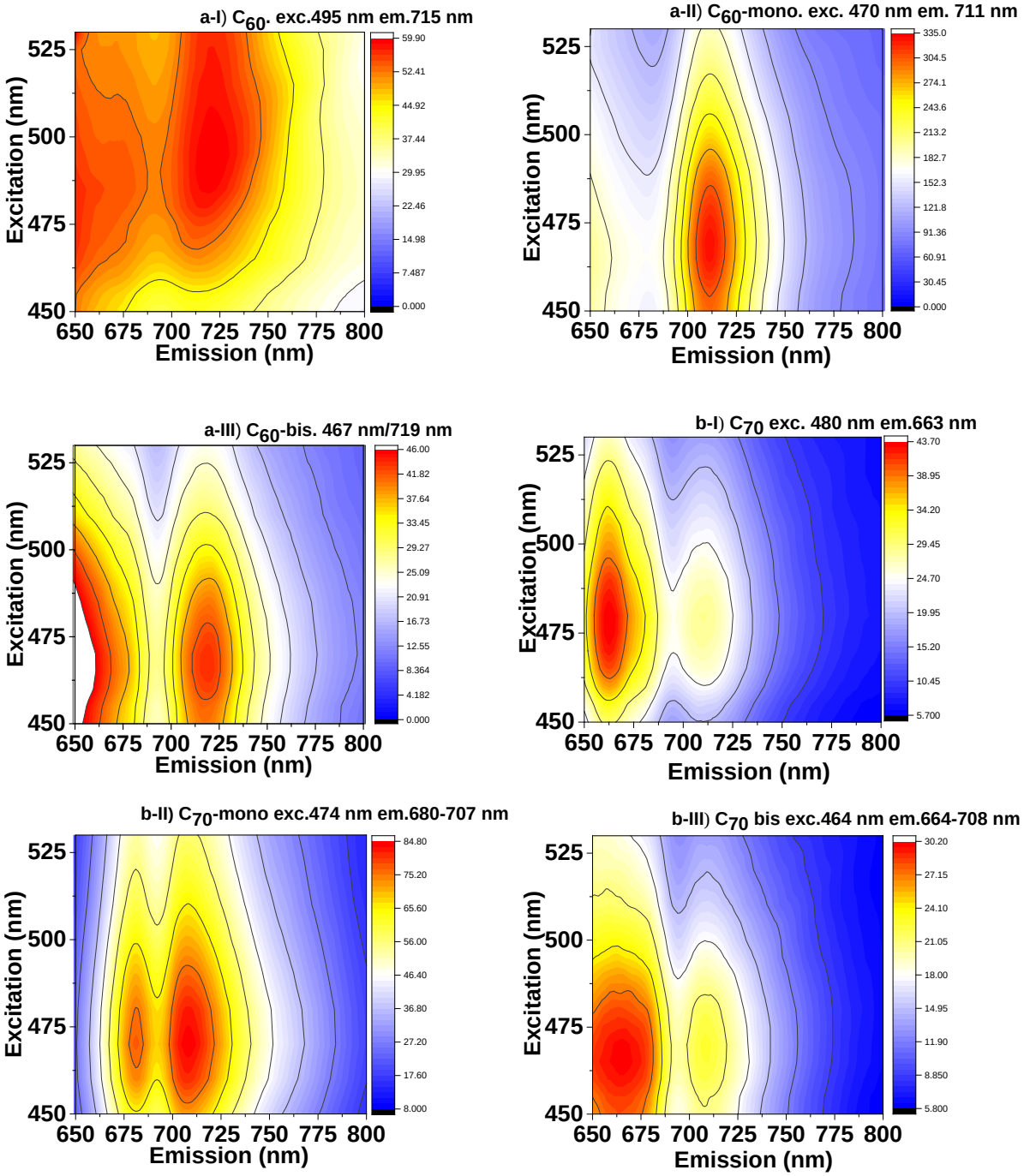

Figure 7. Photoluminescence excitation spectroscopy maps corresponding in the S_1-S_0 fullerene cage transition for a) C_{60} b) C_{70} derivatives in toluene solutions.

The mono and bis adducts of C_{70} exhibit a similar behavior to C_{60} (Figure 7b) as low-lying electronic states are also present in C_{70}. C_{70} therefore exhibits singlet and triplet properties very similar to those of C_{60}. When moving to mono and bis functionalized molecules the $S_1 \rightarrow S_0$ transition is red shifted to 707 nm (1.753 eV) for the mono adduct compared to the pristine C_{70} peak at 667 nm (1.859 eV). Similarly with C_{60}, the optimum λ_{ex}

was now located in lower wavelengths, i.e. higher energy. This emission appears at lower wavelengths than in the C_{60} analogues due to the lower symmetry and reduced electron delocalization of the C_{70} cage. A four-fold increase in the quantum yield of the C_{60}-mono ($9 \cdot 10^{-4}$) compared to C_{60} was observed. However, the opposite effect was observed in C_{70}-mono, with an approximately two-fold decrease compared to pristine C_{70}. All functionalized fullerene systems displayed a large reduction in quantum yield compared to the 1-pyrene carboxaldehyde at the pyrene excitation wavelength. We summarize these findings in Table 2.

Reference	Quantum yield	Sample (excitation)	Quantum yield
Pyrene in ethanol (335 nm)	0.65 (65 %)	**C_{60}-mono (335 nm)**	0.01 (1%)
Pyrene in toluene (335 nm)	0.19 (19 %)	**C_{70}-mono (335 nm)**	0.0012 (0.12%)
C_{60} (520 nm)	$2.2 \cdot 10^{-4}$ (0.022 %)	**C_{60}-mono (520 nm)**	$9 \cdot 10^{-4}$ (0.09 %)
C_{70} (520 nm)	$5.4 \cdot 10^{-4}$ (0.054 %)	**C_{70}-mono (520 nm)**	$3 \cdot 10^{-4}$ (0.03 %)

Table 2. A summary of the quantum yields for two different excitation wavelengths (335 targeting the pyrene and 520 nm targeting the cage).

4.6. Singlet oxygen generation (1270 nm) and NIR (850-1000 nm) photoluminescence

Reactive oxygen species like the singlet oxygen ($^1\Delta_g$), have been proposed as excellent candidates for photodynamic therapy, which is an efficient way to treat cancer cells due to the high reactivity of the excited oxygen molecules. Due to their intersystem crossing, fullerenes are considered among the most efficient photosensitizers [34]. Other photosensitizing systems include macrocycles like porphyrin and pthalocyanin molecules [35] and lately, ultra-small carbon dots [36]. The mechanism is well studied and includes the formation of an intermediate complex between the photensitizer and oxygen, which is subsequently deactivated. This explains the experimental observation of photo sensitized phosphorescence at 1270 nm (0.97 eV).

To study this effect, we initially recorded the photoluminescence excitation spectroscopy maps for pristine C_{60} (Figure 8) and C_{70} (Figure 9) in two different concentrations, 0.03 and 0.3 mg/ml, both measured in CS_2. In order to study the photocycle

process we recorded the NIR emission carbon disulfide solution, since toluene is quenching the singlet oxygen generation due to formation of toluene radicals. We present the measurements in toluene solutions in Figure S10 (S.I). In general singlet oxygen interacts strongly with C-H and O-H bonds. [37] In the CS_2 solutions of the pristine fullerenes, only the singlet oxygen emission is observed with substantial intensity in both cases, without any other NIR radiative decays. By considering the maximum intensity of the 1270 nm peak, it appears that the C_{70} is a more efficient photosensitizer than C_{60} at these two concentrations with CS_2 as the solvent. As we have already presented in Figure 6 the triplet state of the C_{70} has a significantly longer lifetime T_T=130 μs with a quantum yield of ϕ_T=0.9 while for the C_{60} the respective values are T_T=40 μs and ϕ_T=0.96. We note that two different excitation maxima are observed for C_{60} which are concentration independent, in contrast only one maxima is observed for C_{70}.

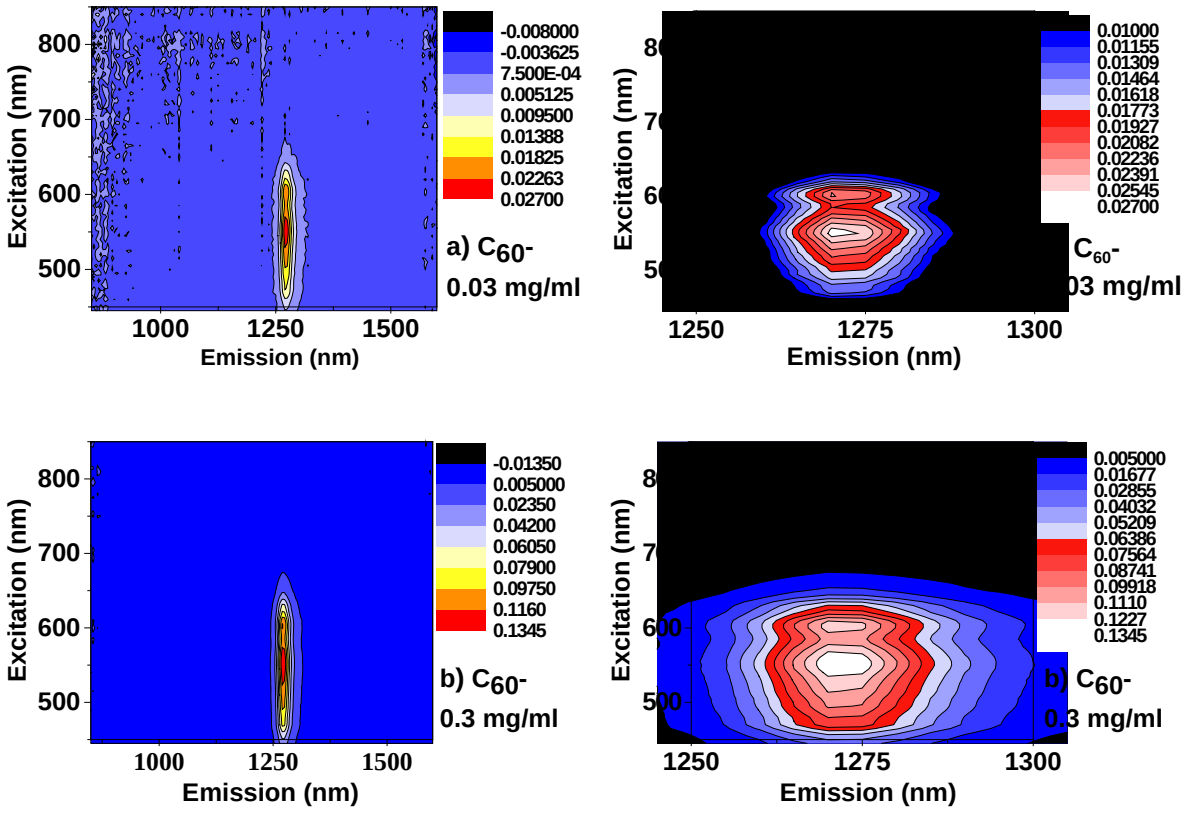

Figure 8. Photoluminescence excitation spectroscopy maps in the region 850-1600 cm^{-1} (left) and a magnification focusing on the 1250-1300 cm^{-1} region of the singlet oxygen phosphorescence (right) for pristine C_{60} dissolved in carbon disulfide. Concentration 0.03 mg/ml (a) and 0.3 mg/ml (b).

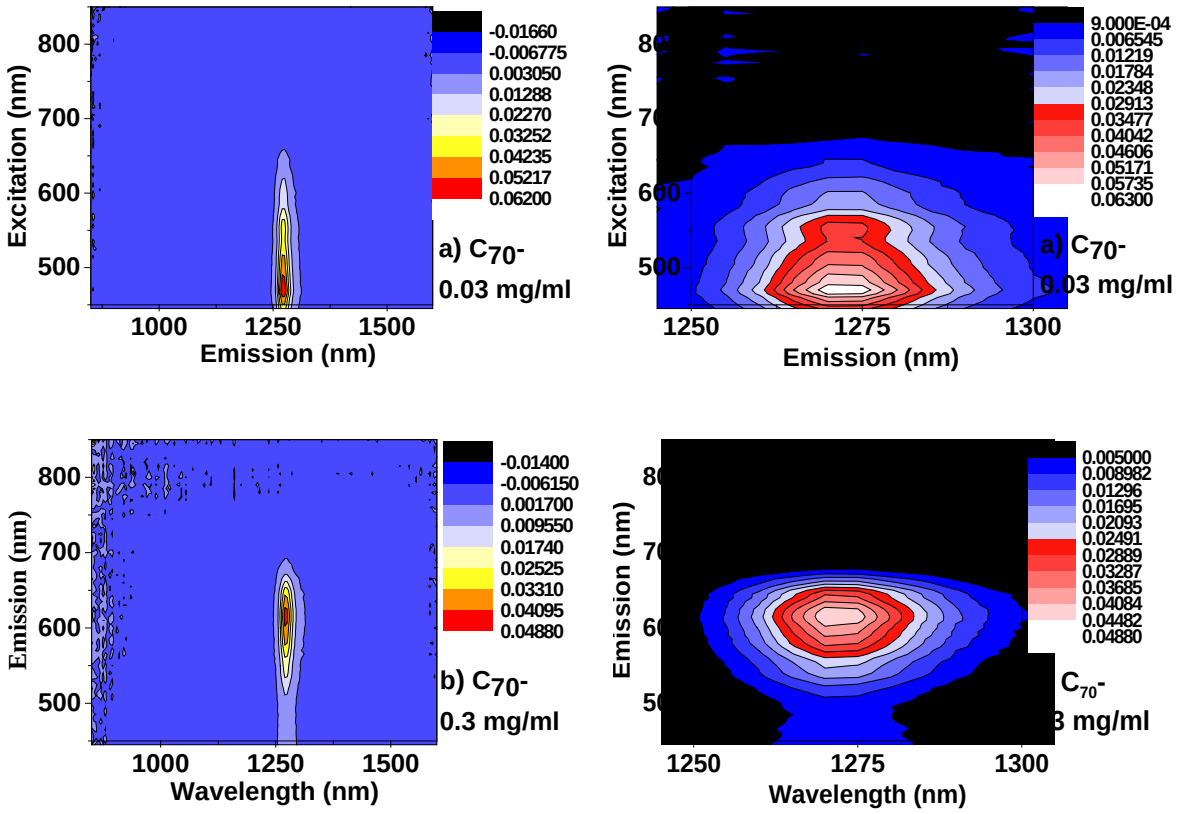

Figure 9. Photoluminescence excitation spectroscopy maps in the range of 850-1600 cm^{-1} (left) and a magnification focusing on the 1250-1300 cm^{-1} region (right) for pristine C_{70} dissolved in carbon disulfide. Concentration 0.03 mg/ml (a) and 0.3 mg/ml (b).

In Figure 10 we present the photoluminescence excitation spectroscopy maps for all of the pyrene functionalized samples in the NIR region where singlet oxygen phosphorescence is observed (range: 850-1350 cm^{-1}). This emission in our samples follows a similar trend to the decay lifetimes, with the C_{60}-mono and C_{70}-bis displaying similar behavior to each other, while the opposite behavior seen in C_{60}-bis and C_{70}-mono (for the time resolved spectroscopy see Figure 5 and 6). In this measurement, the singlet oxygen signal appears with significant intensity in the C_{60}-bis and the C_{70}-mono adducts and is suppressed in the C_{60}-mono and C_{70}-bis adducts.

The presence of charge separation states in fullerene donor-acceptor systems can lead to a charge recombination and overpopulation in the triplet state [38]. Since the photosensitization of the oxygen originates from an energy transfer through the triplet state, we assign the particularly strong intensity of the singlet oxygen to the presence of a long lived, charge separated state. Conversely, when the singlet oxygen is suppressed for C_{60}-

mono and C_{70}-bis adducts, the intersystem crossing transition is forbidden, resulting in the increased quantum yield of the $S_1 \rightarrow S_0$ transition.

The excitation wavelength corresponding to the maximum singlet oxygen generation is 470 nm for all samples with the exception of C_{70}-mono, which is located at 554 nm, meaning a different excitation is leading to the photocycle process. It is also notable that there is a low energy transition in the 800-1000 nm region of the C_{70} samples, indicating a different population and density of states compared to the C_{60} [39]. These are the well-known phosphorescence peaks of C_{70} arising from a decay through the lowest triplet state. [40] They appear much weaker in the pristine C_{70} as can be seen in Figure 9b compared to the two adducts. They also have an opposite counterbalancing trend with the 1270 nm phosphorescence in the pristine, mono and bis adducts samples.

Based on these observations, it will therefore be of interest to further expand this concept in larger fullerene cages like empty cage C_{84} and endohedral metallofullerenes (EMFs). In these systems is it expected that different interactions between the pyrene ring and the fullerene cage will take place. The EMFs can hold up to 6 electrons as donated from the encapsulated metals, allowing for new emission, photocycle and photosensitizing patterns to be observed according to the change in the HOMO LUMO levels and the electron accepting ability.

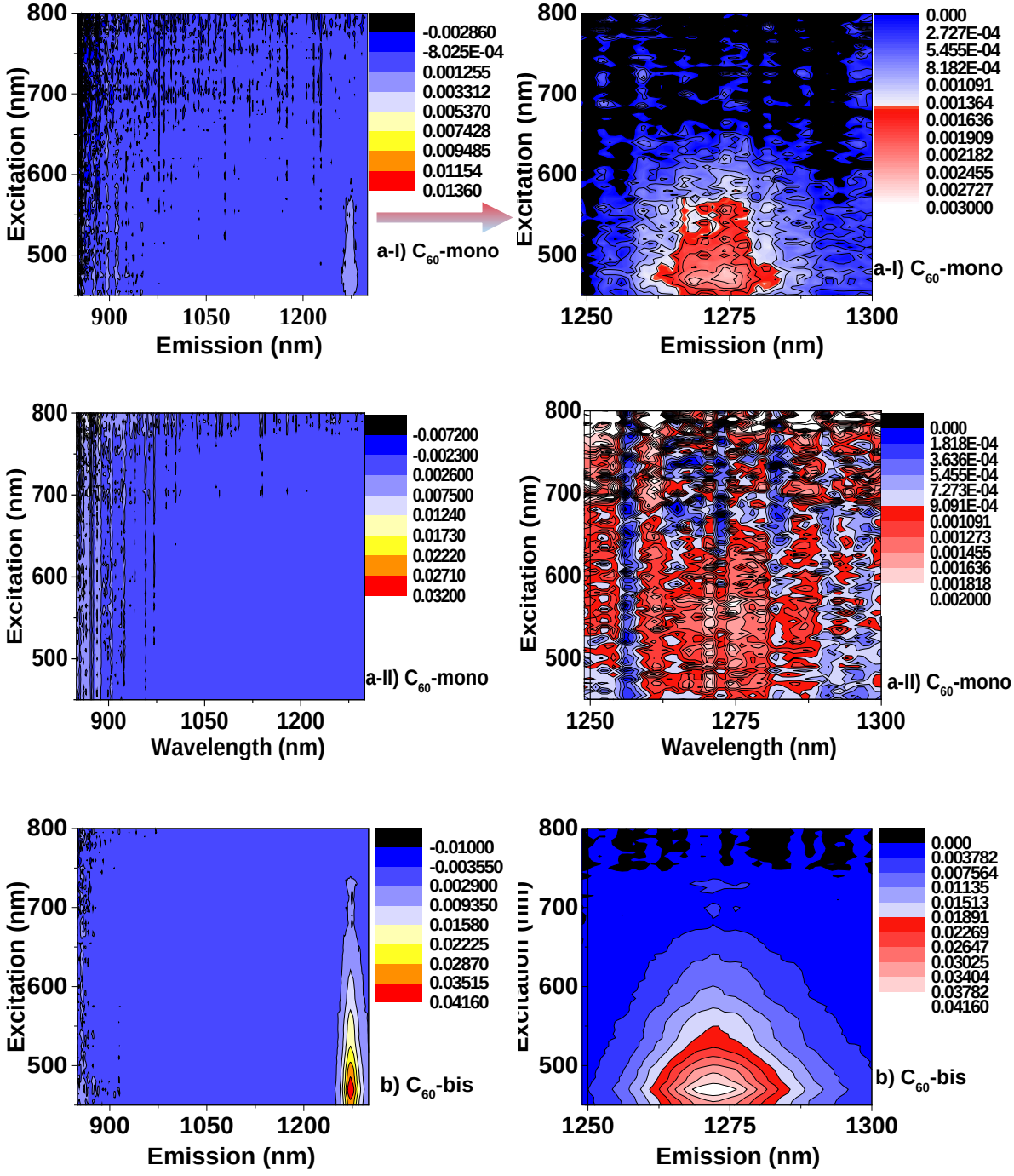
Excitation (nm)
Emission (nm)
-0.002860
-8.025E-04
0.001255
0.003312
0.005370
0.007428
0.009485
0.01154
0.01360
a-I) C60-mono
0.000
2.727E-04
5.455E-04
8.182E-04
0.001091
0.001364
0.001636
0.001909
0.002182
0.002455
0.002727
0.003000
a-I) C60-mono
Wavelength (nm)
-0.007200
-0.002300
0.002600
0.007500
0.01240
0.01730
0.02220
0.02710
0.03200
a-II) C60-mono
0.000
1.818E-04
3.636E-04
5.455E-04
7.273E-04
9.091E-04
0.001091
0.001273
0.001455
0.001636
0.001818
0.002000
a-II) C60-mono
-0.01000
-0.003550
0.002900
0.009350
0.01580
0.02225
0.02870
0.03515
0.04160
b) C60-bis
0.000
0.003782
0.007564
0.01135
0.01513
0.01891
0.02269
0.02647
0.03025
0.03404
0.03782
0.04160
b) C60-bis

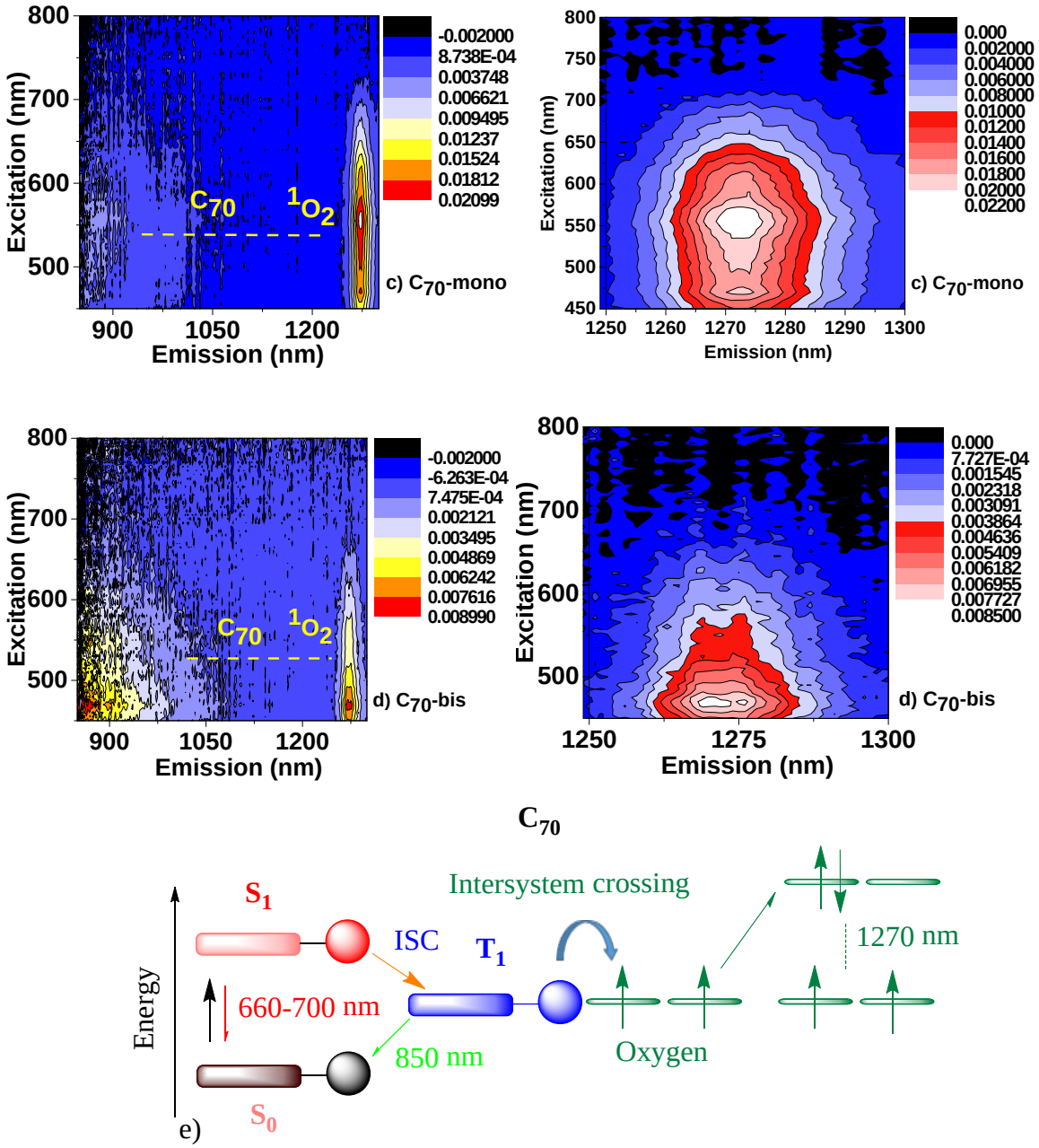

Figure 10. Photoluminescence excitation spectroscopy maps. The right map in each case is the magnification of the 1250-1300 cm^{-1} region where the singlet oxygen emission takes place, with color corresponding to different relative heights. a.I-II) C_{60}-mono adduct in two different concentrations, with the sample used in (a-I) twice as concentrated as the sample in (a-II). Maximum intensity of the singlet oxygen emission: 474 nm b) C_{60}-bis, maximum 470 nm c) C_{70}-mono, maximum 556 nm and d) C_{70}-bis, maximum 470 nm e) The transitions resulting in the NIR and singlet oxygen emission for the C_{70} derivatives.

5. **Conclusions**

The optical and photosensitizing properties of donor-acceptor pyrene-fullerene dyads were found to be influenced not only by the number of pyrene rings attached to the surface, but

also by the size and shape of the fullerene cage, observed with C_{60} and C_{70}. Charge transfer from the pyrene to the electron accepting fullerene was demonstrated by observing the quenching of the fullerene PL emission. When a second pyrene unit was attached there was a substantial change in the fluorescence lifetimes associated with both the pyrene and the fullerene. Opposite trends were observed in the decay mechanism, the quantum yields, and the photosensitizing properties of C_{60}-mono and C_{70}-bis compared to C_{60}-bis and C_{70}-mono. This signals an influence from the fullerene cage on the intramolecular electron transfer and on the formation of locally excited against charge separation states, with different numbers of pyrene containing units required to observe the same effect. This competition between locally excited and charge separated states was further confirmed by employing a solvent with higher dielectric constant through small shifts and minor loss of fine features. NIR 3D mapping also showed the same trend: C_{60}-mono and C_{70}-bis both displayed a quenching of the singlet oxygen signal, while C_{60}-bis and C_{70}-both acted as strong photosensitizers for singlet oxygen. These adducts are therefore among the best choices for photogeneration of the excited singlet oxygen state $^1O_2$.

ACKNOWLEDGMENT. We thank Dr. Edward A. Laird for useful discussions. We thank Ms Karolina Korzyska and Prof. Harry Anderson for providing access to the photoluminescence spectrometer. We acknowledge EPSRC funding for the Fellowship programme ‘Manufacturing the future: endohedral fullerenes, small molecules, big challenges’ (EP/K030108/1).).

Electronic Supplementary Information (ESI) available: Blank toluene spectra indicating the excitation dependent Raman peaks, mass spectra for the bis adducts, ^{1}H NMR spectra and UV-Visible absorbance and photoluminescence spectra of the pristine pyrene and the excitation dependent NIR photoluminescence maps in toluene, the photoluminescence maps under $\lambda_{exc=}$.300-450 nm in chloroform solutions and the residual fitting data and instrument response function for the bi-exponential decay curves are available free of charge via the internet.

References

1. R.Sijbesma, G.Srdanov, F.Wudl, J.A.Castoro, C.Wilkins, S.H.Friedman, D.L.DeCamp, G.L.Kenyon. J.Am.Chem.Soc. 115 (1993) 6510

2. Y. Yamakoshi, N.Umezawa, A.Ryu, K.Arakane, N.Miyata, Y.Goda, T. Masumizu, T,Nagano. J.Am.Chem.Soc. 125(42) (2003) 12803

3.a) Y.He, Y.Li. Phys.Chem.Chem.Phys. 13 (2011) 1970 b) S-H,Liao, H-J,Jhuo, Y-S. Cheng, S-A. Chen. Adv.Mater. 25 (2013) 4766

4. S.R.Plant, M.Jevric, J.J.L.Morton, A.Ardavan, A.N.Khlobystov, G.A.D. Briggs, K.Porfyrakis. Chem.Sci. 4 (2013) 2971

5. a) K.Kordatos, S.Bosi, T.Da Ros, A.Zambon, V.Lucchini, M.Prato. J.Org.Chem. 66 (2001) 2802 b) M.Taki, S.Sugita, Y.Nakamura, E. Kasashima, E.Yashima, Y.Okamoto, J.Nishimura J.Am.Chem.Soc. 119 (1997) 926

6. S.Aroua, Y.Yamakoshi. J.Am.Chem.Soc. 134 (2012) 20242

7. Z.A.Page, Y.Liu, V.V.Duzhko, T.P.Russell, T.Emrick. Science 346 (2014) 441

8. M.Gallego, J. Calbo, J. Arago, M.R.K.Calderon, F.H. Liquido, T. Iwamoto, A.K. Greene, A.A.Jackson, E.M.Perez, E.Orti, D.M. Guldi, L.T.Scott, N.Martin. Angew.Chem.Int.Ed. 53 (2014) 2170

9. a) M.B. Zimmt, D.H.Waldeck. J.Phys.Chem.A. 107 (2003) 3580 b) A.Kahnt, J.Karnbratt, L.J.Esdaile, M.Hutin, K.Sawada, H.L.Anderson, B.Albinsson. J.Am.Chem. Soc. 133 (2011) 9863–9871 c) K.A. Zachariasse, S.I. Druzhinin, S.A. Kovalenko, T.Senyushkina J. Chem. Phys. 131, (2009) 224313

10. I.D.Petsalakis, G.Theodorakopoulos. Chem.Phys.Lett. 466 (2008) 189-196

11. C.K.Tai, W.Y.Hsieh, P.L.Yeh, H.L.Chiu, B.C.Wang. J. Chin. Chem. Soc. 60 (2013) 251-260

12. a) T. Numata, T.Murakami, F.Kawashima, N.Morone, J.E.Heuser, Y. Takano, K. Ohkubo, S. Fukuzumi, Y. Mori, H. Imahori. J.Am.Chem.Soc. 134 (2012) 6092 b) L.Chen, Y.Honsho, S.Seki, D.Jiang. J.Am.Chem.Soc. 132 (2010) 6742 c) T.O'Connor, M.S.Panov, A.Mereschenko, A.N.Tarnovsky, R.Lorek, D.Perera, G.Diederich, S.Lambright, P.Moroz, M.Zamkov. ACS Nano 6 (2012) 8156

13. J.W.Aborgast, A.P. Darmanyan, C.S.Foote, F.N.Diederich, Y.Rubin, F.Diederich, M. Alvarez, S.J. Anz, R.L. Whetten. J.Phys.Chem. 95 (1991) 11

14. K. Hutchison, J. Gao, G. Schick, Y.Rubin, F. Wudl. J.Am.Chem.Soc. 121 (1999) 5611.

15. V. Filidou, S.Simmons, S.D.Karlen, F.Giustino, H.L.Anderson, J.J.L. Morton. Nat.Phys. 8(8) (2012) 596

16. Ya-Ping Sun, Ping Wang, Norwood B. Hamilton J. Am. Chem. Soc. 115 (1993) 6378-6381

17. D.Milic, M. Prato. Eur.J.Org.Chem. 2010, 476

18. M.I.Sluch, I.D.W.Samuel, M.C.Petty. Chem.Phys.Lett. 280 (1997) 315

19. R.B.Martin, K.Fu, Y-P.Sun. Chem.Phys.Lett. 375 (2003) 619

20. D.M.Guldi, F.Spanig, D. Kreher, I.F.Perepichka, C.Van der Pol, M.R. Bryce, K.Ohkubo, S.Fukuzumi. Chem.Eur.J. 14 (2008) 250

21. P.Lianos, G.Cremel. Photochemistry and Photobiology. 429 (2008) 429

22. a) L.Pineiro, M.Novo, W.Al-Soufi. Adv.Coll.Int.Sci. 215 (2015) 1-12 b) G.Bains, A.B.Patel, V. Narayanaswami. Molecules 16 (2011) 7909-7935 c) D. S. Karpovich, G. J. Blanchard J. Phys. Chem. 99 (1995) 3951-3958

23. W.Andreoni, F.Gygi, M.Parrinello. Chem.Phys.Lett. 189(3) (1992) 241

24. S.R.Wilson, Q.Lu. J.Org.Chem. 60 (1995) 6496

25. S.Olsen. J. Phys. Chem. B 119 (2015) 2566−2575

26. B. Bernardo, D. Cheyns, B. Verreet, R.D. Schaller, B.P. Rand, N.C. Giebink. Nat.Comm. 5, (2014), 2345

27. M.Lee, O-K.Song, J-C.Seo, D.Kim, Y.D.Suh, S.M.Jin, S.K.Kim. Chem.Phys.Lett. 196(3,4) (1992) 325

28. Y.P.Sun, G.E.Lawson, J.E.Riggs, B.Ma, N.Wang, D.K.Moton. J.Phys.Chem.A. 102 (1998) 5520

29. G.Schick, M.Levitus, L.Kvetko, B.A.Johnson, I.Lamparth, R.Lunkwitz, B.Ma, S.I.Khan, S.A.Garcia-Garibay, Y.Rubin. J.Am.Chem.Soc. 121 (1999) 3246

30. Z.J.Li, W.W.Yang, Z.Gao. J.Phys.Chem.A. 115 (2011) 6432

31. D.M.Guldi, K.D.Asmus. J.Phys.Chem.A. 101 (1997) 1472

32. T.Gareis, O.Kothe, J.Daub. Eur.J.Org.J. 1549 (1998)

33. A.S.D.Sandanakaya, Y.Araki, O.Ito, G.R.Deviprasad, P.M.Smith, L.M. Rogers, M.E.Zandler, F.D. D'Souza. Chem.Phys. 325 (2006) 452

34. a) A. A. Krasnovsky, KV. Neverov Biophysics 55 (2010) 349–352 b) Y.Yamakoshi, S.Sueyoshi, K.Fukuhara, N.Miyata. J.Am.Chem.Soc. 120 (1998) 12363-12364 b) J.Wang, J.Leng, H.Yang, G.Sha, C.Zhang. Langmuir 29 (2013) 9051-9056

35. J.F.Lovell, T.W.B.Liu, J.Chen, G.Zheng. Chem.Rev. 110 (2010) 2839

36. J.Ge et al. Nat.Commun. 5 (2014) 4596

37. F.Wilkinson, W.P.Helman, A.B.Ross. J. Phys. Chem. Ref. Data 24 (1995) 663

38. B.P. Karsten, R.K.M. Bouwer, J.C. Hummelen, R.M. Williams, R.A.J. Janssen. Photochem. Photobiol. Sci. 9 (2010) 1055–1065

39. Mario N. Berberan-Santos, Joa˜o M. M. Garcia J. Am. Chem. Soc. 118 (1996) 9391-9394

40. A. Sassara, G. Zerza, M. Chergui J. Phys. Chem. A 102 (1998) 3072-3077